ORIGINAL ARTICLE

Conserved Immune Activation and Compartment-Specific Dysregulation in Temporomandibular Joint Osteoarthritis Cartilage: A Cross-Species Transcriptomic Analysis

Dedi Sucipto[1*], Cindy Susanti[2], Vidhya Sathyakirti[3]

[1] Department of Internal Medicine, Phlox Institute, Palembang, Indonesia
[2] Department of Internal Medicine, Provita Hospital, Jayapura, Indonesia
[3] Department of Radiology, Queensland State Hospital, Queensland, Australia

ARTICLE INFO

ARTICLE TYPE
Original Article

ARTICLE HISTORY
Received: November 5, 2025
Accepted: December 2, 2025
Published: December 30, 2025

KEYWORDS
Cartilage; Differential gene expression; Osteoarthritis; Temporomandibular joint; Transcriptomics

CORRESPONDING AUTHOR
Dedi Sucipto
E-mail: Dedi.sucipto@phlox.or.id
ORCID: 0009-0009-1369-8317

DOI
https://doi.org/10.59345/crown.v3i2.329

ABSTRACT

Background: Temporomandibular joint osteoarthritis (TMJ-OA) is molecularly heterogeneous, and differences in tissue, species, and disease model complicate transcriptomic integration.

Objective: This study aimed to identify conserved and compartment-specific transcriptional programs across complementary rabbit and rat TMJ-OA cartilage datasets.

Methods: A targeted GEO screen identified rabbit post-traumatic TMJ-OA (GSE232867; paired condylar cartilage and superficial zone; three animals per condition) as the primary dataset and rat unilateral anterior crossbite TMJ-OA (GSE207461; three samples per condition) for pathway-level validation. Counts were filtered with edgeR, TMM-normalized, transformed with voom, and modeled with limma; rabbit analyses were blocked by animal. Differentially expressed features required BH-FDR < 0.05 and absolute log2 fold change >= 1. Ordered g:Profiler enrichment tested directional pathway concordance.

Results: Rabbit condylar cartilage yielded 421 differentially expressed features (346 upregulated and 75 downregulated), the superficial zone yielded 180 (69 upregulated and 111 downregulated), and 135 showed a condition-by-compartment interaction. Immune-associated genes were prominent in condylar cartilage, whereas superficial-zone downregulation centered on mitotic programs. Only Morf4l2 met the strict rat threshold, but 13 upregulated pathways were concordant across species; leukocyte activation was strongest (conservative adjusted P = 2.16 x 10^-6).

Conclusion: Pathway-level immune activation was the most reproducible signal across these animal TMJ-OA cartilage datasets, accompanied by compartment-specific proliferative dysregulation. Small preclinical bulk datasets preclude cell-specific or human inference.

1. Introduction

Temporomandibular joint osteoarthritis (TMJ-OA) is a progressive disorder of the mandibular condyle and associated joint tissues that can cause pain, crepitus, functional limitation, and structural deterioration. Unlike hyaline cartilage in many appendicular joints, the mandibular condyle contains fibrocartilaginous and zone-specific cellular compartments exposed to complex mechanical loading. Its disease biology therefore integrates mechanical injury, extracellular-matrix remodeling, subchondral-bone responses, inflammation, and disturbed chondrocyte homeostasis [1-3].

The temporomandibular joint is structurally and functionally distinct from most synovial joints. Its articular surface is covered by fibrocartilage, it operates under combined rotational and translational movement, and it continuously adapts to occlusal loading. Degeneration can therefore arise through interacting mechanical, inflammatory, and reparative processes rather than through a single linear pathway. Histopathologic progression includes matrix disorganization, surface fibrillation, altered chondrocyte behavior, remodeling of the subchondral compartment, and variable synovial or neurovascular responses. These processes help explain why clinical symptoms, structural imaging, and molecular activity do not always progress in parallel and why molecular markers obtained from one tissue or disease stage may not generalize to another [1-3].

Cellular organization within the mandibular condyle further complicates biological interpretation. The superficial zone is positioned at the mechanically exposed interface and contains cells implicated in surface maintenance and repair, whereas deeper condylar cartilage compartments contain more differentiated chondrocyte populations embedded in a distinct extracellular matrix. A disease-associated transcript detected in whole tissue may consequently reflect altered transcription within resident cells, a change in the relative abundance of cell populations, vascular or blood content, immune-cell recruitment, or several of these mechanisms simultaneously. Analyses that preserve compartment information are therefore better suited to distinguish shared disease responses from spatially restricted programs, even though bulk sequencing cannot assign those programs to individual cell types [4-7].

High-throughput transcriptomics can identify coordinated molecular programs beyond single-marker observations. However, available TMJ-OA datasets differ in species, disease induction, tissue compartment, time point, and statistical power. Strict gene lists may consequently fail to overlap even when broader biological pathways are shared. An integrative analysis should therefore preserve study-specific contrasts, control false discovery, account for repeated sampling, and test concordance at both feature and pathway levels [8,9].

This distinction between feature-level and pathway-level reproducibility is important in small preclinical studies. With only a few biological replicates, an individual

transcript must show a comparatively large and stable effect to remain significant after genome-wide multiplicity correction. A second dataset may contain a biologically related but smaller shift that does not cross the same threshold. Requiring strict overlap of dichotomized gene lists can therefore produce a false impression of biological disagreement. Rank-based enrichment provides a complementary test because it evaluates whether many members of a functional program move coherently in the same direction, while still allowing each experiment to retain its own scale and variance structure. Agreement at the pathway level is not equivalent to replication of every gene, but it can identify biological signals that are more robust to model-specific noise.

Cross-species integration also requires restraint. Rabbit and rat models differ in anatomy, disease induction, sampling, genome annotation, and the mapping of gene identifiers. Direct pooling would treat nonexchangeable observations as though they arose from one experiment and would obscure rather than resolve heterogeneity. A defensible alternative is to analyze each dataset independently, align annotated symbols only for supportive comparisons, and require directional agreement of enriched pathways. Human single-cell studies can then provide contextual evidence about candidate cellular sources without being used as a substitute for a replicated human bulk cartilage comparison [4,8].

The Gene Expression Omnibus (GEO) provides public study metadata and expression matrices suitable for secondary analysis. A targeted candidate screen identified a rabbit post-traumatic model with paired condylar-cartilage and superficial-zone profiles and an independent rat mechanical-malocclusion model with direct condylar-cartilage counts [10,11]. Recent multi-omics and patient-specific progression-modeling investigations provide complementary context but do not replace direct replication of these bulk-cartilage contrasts [12,13]. Human single-cell work is also biologically informative, but no adequately replicated healthy-versus-OA human bulk condylar-cartilage count dataset met the present analytical-role criteria [4,8].

The rabbit dataset was particularly informative as a primary dataset because the same animals contributed profiles from both condylar cartilage and the superficial zone. That pairing supports explicit modeling of within-animal dependence and a condition-by-compartment interaction. The rat dataset, although smaller and heterogeneous, was biologically independent: osteoarthritis was induced through unilateral anterior crossbite rather than post-traumatic injury, and condylar cartilage was collected after eight weeks of modeling. Concordance across these nonidentical systems would therefore support a conserved response at the level tested, whereas discordance could reveal model-, species-, or compartment-specific biology [10,11].

An unresolved analytical gap was thus not the absence of individual TMJ-OA transcriptomic studies, but the absence of a transparent integration that simultaneously preserved the paired rabbit compartments, enforced false-discovery control, distinguished annotated genes from tested features, and evaluated cross-species agreement without pooling incompatible count matrices. Addressing this gap could clarify which signals are strong within the rabbit model, which are restricted to a cartilage compartment, and which retain directionally consistent pathway evidence in a second species.

The novelty of this study lies in combining a paired, compartment-aware analysis of rabbit TMJ-OA cartilage with a direction-aware test of pathway reproducibility in an independent rat model, while explicitly separating strict feature-level evidence from ranked pathway-level concordance. The primary aim was to identify differentially expressed features and enriched biological pathways in rabbit TMJ-OA condylar cartilage. The secondary objectives were to characterize superficial-zone responses, test the condition-by-compartment interaction, quantify supportive cross-species concordance among shared gene symbols, and determine whether upregulated or downregulated pathways were directionally replicated in rat condylar cartilage.

2. Methods

Study design and targeted dataset selection

This secondary targeted integrative study used public, de-identified GEO data. An NCBI E-utilities query executed on 5 August 2025 returned 34 candidate records. Selection was role based rather than intended as a systematic review: the primary dataset required replicated bulk counts and paired cartilage compartments, whereas pathway-level validation required a biologically independent species/model, directly sampled condylar cartilage, an untreated disease-control contrast, downloadable gene-level counts, and at least three biological replicates per group. Records centered on synovium, saliva, articular disc, subchondral bone, cell culture, single-cell/spatial profiling, genetic or therapeutic perturbations, parent accessions, or under-replicated contrasts were excluded. GSE232867 fulfilled the primary role and GSE207461 fulfilled the validation role; the full screening log accompanies the analysis archive.

The executed search was: ((temporomandibular joint[All Fields] OR condylar cartilage[All Fields]) AND (osteoarthritis[All Fields] OR degeneration[All Fields]) AND (expression profiling by high throughput sequencing[DataSet Type] OR expression profiling by array[DataSet Type])). Candidate accession records and linked Series metadata were reviewed against the prespecified analytical roles. Exclusion was based on tissue, experimental unit, contrast, replication, availability of gene-level counts, and whether an accession represented an independent experiment rather than a parent or linked record. The purpose was analytical compatibility, not exhaustive evidence synthesis; accordingly, no PRISMA-style claim, risk-of-bias grading, or systematic-review registration was applied.

The primary role required more than a conventional disease-control comparison because the study question included compartment specificity. GSE232867 uniquely combined replicated bulk count data with matched profiles from two cartilage compartments in each rabbit. The validation role used a different standard: a second dataset did not need paired compartments but had to provide direct condylar-cartilage counts from an untreated osteoarthritis-control comparison in another species or model. GSE207461 met that requirement. These role definitions were fixed before the final integration outputs were interpreted, and every screened record, decision, and

exclusion reason was retained in the machine-readable screening log.

Included datasets

GSE232867 profiled condylar cartilage (CC) and the superficial zone (SZ; labeled fibrocartilage in the deposited workbook) from a rabbit post-traumatic TMJ-OA model and matched controls. Three animals per condition contributed both compartments, producing 12 tissue profiles. GSE207461 profiled rat condylar cartilage after unilateral anterior crossbite induction and in normal controls, with three samples per condition. Because species and induction mechanisms differed, count matrices were analyzed separately rather than pooled.

For GSE232867, the deposited sample titles identified control and osteoarthritis states, biological replicates 1-3, and either condylar-cartilage or superficial-zone cells. The resulting factorial structure comprised control CC, control SZ, OA CC, and OA SZ, with three observations in each group and a shared animal identifier across compartments. GEO metadata report RNA extraction with the RNeasy Micro kit, ribosomal-RNA depletion, directional library preparation, quality assessment with MultiQC, adapter and quality trimming with Trim Galore, STAR-based alignment, StringTie-assisted transcriptome assembly against the rabbit OryCun2.0 reference, and Salmon quantification. The present study did not reprocess raw sequence reads; it analyzed the deposited gene-level raw-count columns and used the accompanying annotation fields supplied by the original investigators [10].

For GSE207461, the deposited Series and sample records identified three Sprague-Dawley control samples and three unilateral-anterior-crossbite samples collected after eight weeks of modeling. GEO metadata describe Trizol RNA extraction, Illumina library preparation and paired-end sequencing, Cutadapt filtering, FastQC assessment, and annotation against rat Ensembl version 101. The supplementary workbook contained both expression summaries and columns matching the deposited count.* naming pattern; only those gene-level count columns were used for differential-expression modeling. The dataset was not treated as a technical replication of the rabbit experiment because its species, induction mechanism, time point, sequencing workflow, and tissue dissection were independent [11].

No sample was removed from either dataset. Sample labels in the matrices were reconciled with the Series metadata before group assignment. The biological unit was the animal for the rabbit dataset and the deposited biological sample for the rat dataset. Because the rabbit compartments originated from the same animals, treating all 12 profiles as independent would underestimate uncertainty; the analysis therefore retained animal identity as a blocking factor. The rat design contained one tissue profile per sample and required no repeated-measures block.

Matrix acquisition and quality control

Official supplementary workbooks and Series metadata were downloaded from NCBI GEO. The GSE232867 workbook stored complete data but had a malformed worksheet dimension that caused ordinary readers to return only cell A1; the explicit range A1:AZ14623 was recovered, reconciled against metadata, and exported through reproducible code. Rat counts were read from the deposited count.* columns. Matrices were checked for sample-label concordance, missing values, negative values, non-integer counts, duplicated identifiers, and library-size anomalies. No missing, negative, or non-integer counts were present.

The recovered rabbit worksheet contained two header rows followed by 14,621 submitted Ensembl features. Column names were made unique before extraction, and columns beginning with RawCounts_ were converted to numeric values. Rabbit condition was inferred from the deposited sample convention, compartment from the CC or superficial-zone label, and animal identity from the matched replicate code. The rat workbook contained 44,746 submitted feature rows; columns beginning with count. were converted to the count matrix, while gene identifiers, gene names, and transcript-type fields were retained for annotation.

Quality control was deliberately separated into matrix integrity and expression suitability. Matrix-integrity checks counted missing, negative, and non-integer entries, verified the expected number of sample columns, and compared column labels with GEO metadata. Expression suitability was evaluated through library sizes, low-expression filtering, normalized expression distributions, and principal-component structure. No value was imputed, winsorized, or replaced, and no feature was removed on the basis of its observed disease effect. The original downloaded workbooks were preserved unchanged; all derived matrices and tables were produced by script.

Differential-expression analysis

Analyses were performed in R with edgeR, voom, and limma [14-16]. Lowly expressed features were removed with filterByExpr; library composition was normalized with the trimmed mean of M-values (TMM); voom estimated precision weights; and limma fitted linear models. Empirical-Bayes moderation used trend=TRUE to accommodate intensity-dependent variance. For rabbit data, the design represented condition, compartment, and their interaction. Animal identity was a blocking factor and within-animal dependence was estimated with duplicateCorrelation (consensus correlation 0.0587). Prespecified contrasts compared OA with control within CC, OA with control within SZ, and the difference between these contrasts. The rat model compared OA with control.

P values were adjusted with the Benjamini-Hochberg method. A feature was classified as differentially expressed when FDR was <0.05 and absolute $\log_2$ fold-change was ≥1. Differential-expression analysis estimates transcript abundance and does not identify DNA sequence variants.

Low-expression filtering was performed separately within each species because the available feature universes and library depths differed. The filterByExpr function used the corresponding design matrix rather than an arbitrary count cutoff. TMM normalization then estimated sample-specific scaling factors to reduce compositional bias, after which voom transformed counts to $\log_2$ counts per million and estimated the mean-variance relationship required for precision-weighted linear modeling. Principal-component analysis used the normalized voom expression matrix, centered by feature without unit-variance scaling, so that the largest sources of normalized transcriptional variation could be examined without allowing low-variance features to dominate.

For rabbit data, the no-intercept design contained four group means: control CC, control SZ, OA CC, and OA SZ. The OA-versus-control CC contrast was the primary comparison. The corresponding SZ contrast assessed disease-associated change at the surface, and the interaction contrast was calculated as (OA SZ − control SZ) − (OA CC − control CC). A positive interaction therefore indicates a more positive or less negative OA effect in SZ than in CC, whereas a negative interaction indicates relative suppression in SZ. The duplicate-correlation estimate was incorporated into the second voom transformation and the linear fit, preserving the pairing while avoiding an overparameterized animal fixed-effect model for only six animals.

For the rat dataset, a no-intercept two-group design compared unilateral-anterior-crossbite samples with controls. The same filtering, TMM, voom, limma, trend-moderated empirical-Bayes, and Benjamini-Hochberg framework was applied so that inferential thresholds were comparable across species. Nevertheless, effect estimates and residual variances were calculated independently. Moderated statistics were retained for every tested feature, not only threshold-positive results, because the full ranked distributions were required for correlation and enrichment analyses.

Feature-level results were merged with deposited annotation after model fitting. Ensembl identifiers remained the primary keys for rabbit totals, and the term feature is used when reporting threshold counts because some tested identifiers lacked a current nonempty symbol. For gene-level descriptions, rows with usable symbols were selected explicitly. When more than one tested row mapped to the same case-insensitive symbol, the row with the largest absolute moderated t statistic was retained for cross-species ranking. The inclusive absolute $\log_2$-fold-change threshold of at least 1 was applied exactly as written, together with adjusted $P<0.05$.

Functional enrichment and cross-species integration

g:Profiler tested Gene Ontology Biological Process, Reactome, KEGG, and WikiPathways terms using filtered protein-coding symbols as the statistical universe and g:SCS multiple-testing correction. Strict upregulated and downregulated lists were tested separately. Ordered enrichment was also performed on the 5,000 most positive and 5,000 most negative annotated protein-coding features ranked by moderated t statistics. A pathway was considered directionally replicated when it was significant and concordant in both species; the larger adjusted P value served as a conservative replication statistic.

Gene-level cross-species agreement was assessed after deduplicating shared symbols by the largest absolute moderated t statistic. Spearman correlation summarized $\log_2$ fold-change concordance. This symbol-based analysis is supportive and is not equivalent to curated one-to-one orthology mapping.

Two complementary enrichment strategies were used because strict threshold lists and continuous ranks answer different questions. Over-representation analysis of strict rabbit CC and SZ lists asked which functions were concentrated among features meeting both the FDR and fold-change thresholds. Ordered analysis used the signed moderated-t ranking and could detect a coordinated program even when many individual members were below the strict cutoff. Upregulated and downregulated directions were always tested separately; a pathway significant in opposite directions across species was not counted as replication.

Only protein-coding rows with nonempty symbols entered g:Profiler. The custom background for each species was the set of filtered, annotated protein-coding symbols that could have appeared in that analysis, limiting enrichment bias from different detection and annotation universes. Queries were species specific (Oryctolagus cuniculus and Rattus norvegicus), used GO Biological Process, Reactome, KEGG, and WikiPathways, and applied g:Profiler's g:SCS correction at a 0.05 threshold. Raw JSON responses, including the database build information returned by the API, were saved before scalar result tables were generated.

Directional cross-species pathway replication was defined only for GO Biological Process terms significant in both ordered upregulated analyses or both ordered downregulated analyses. Terms were joined by stable GO identifier and name. For each concordant term, the larger of the rabbit and rat adjusted P values was reported as a conservative statistic, ensuring that a very strong signal in one species could not compensate for a weak or nonsignificant result in the other. This statistic was used for ranking replicated pathways rather than as a newly estimated meta-analytic P value.

Reproducibility

Independent scripts recomputed feature filtering, TMM factors, voom models, empirical-Bayes statistics, BH adjustments, DEG flags, cross-species correlations, enrichment intersections, and figures. Code, complete result tables, raw g:Profiler responses, and R session information accompany the manuscript.

The analysis archive separates scripts, complete differential-expression tables, data-quality summaries, PCA coordinates, shared-symbol tables, enrichment outputs, raw API responses, and figure source files. Each differential-expression table contains the model coefficient, average expression, moderated statistic, nominal P value, adjusted P value, annotation, threshold flag, and direction. Session information records the R platform and loaded package versions. The deposited GEO workbooks are referenced by accession rather than redistributed in the supplementary archive, allowing the scripts to be rerun against the authoritative source files.

Numerical values used in the abstract, main text, tables, and figures were reconciled against the machine-readable outputs. Counts were regenerated from the final threshold flags, correlations from the final deduplicated symbol table, and pathway displays from the saved g:Profiler results. Figure files were exported as 300-dpi PNGs for the manuscript and as PDFs for scalable inspection. No result was selected or omitted solely because of statistical significance; complete tables remain available for evaluation of subthreshold effects.

3. Results

Feature retention and sample structure

Filtering retained 14,540 of 14,621 submitted rabbit features and 29,815 of 44,746 submitted rat features. Rabbit library sizes ranged from 7.33 to 16.77 million reads; rat library sizes ranged from 71.52 to 86.52 million.

Principal-component analysis separated rabbit compartments prominently and retained condition-related structure. In the rat dataset, one OA sample was distinct on the second principal component, consistent with within-group heterogeneity.

Thus, 99.4% of submitted rabbit features and 66.6% of submitted rat features passed design-aware expression filtering. The difference in retention reflects the distinct deposited feature universes, count distributions, and sequencing depths rather than application of a common arbitrary abundance threshold. All 12 rabbit and six rat libraries contributed to the final models. Across both matrices, the integrity checks found zero missing, negative, or non-integer count entries, and the sample-label assignments were concordant with the deposited metadata.

In rabbit data, PC1 explained 31.4% of normalized-expression variance and primarily separated CC from SZ profiles, while PC2 explained 21.3% and further distributed samples by condition and individual variation. The strong compartment structure supported retention of compartment-specific contrasts instead of collapsing the 12 profiles into a single OA-control comparison. In rat data, PC1 and PC2 explained 22.6% and 20.6% of variance, respectively. Controls clustered on the negative side of PC1, whereas OA samples shifted toward positive PC1 values; one OA sample also had a substantially higher PC2 score than the other two. This sample was retained because its matrix values and label passed the predefined checks and because removing it solely on PCA appearance would introduce post hoc selection. The complete sample structure and variance distribution are illustrated in Figure 1.

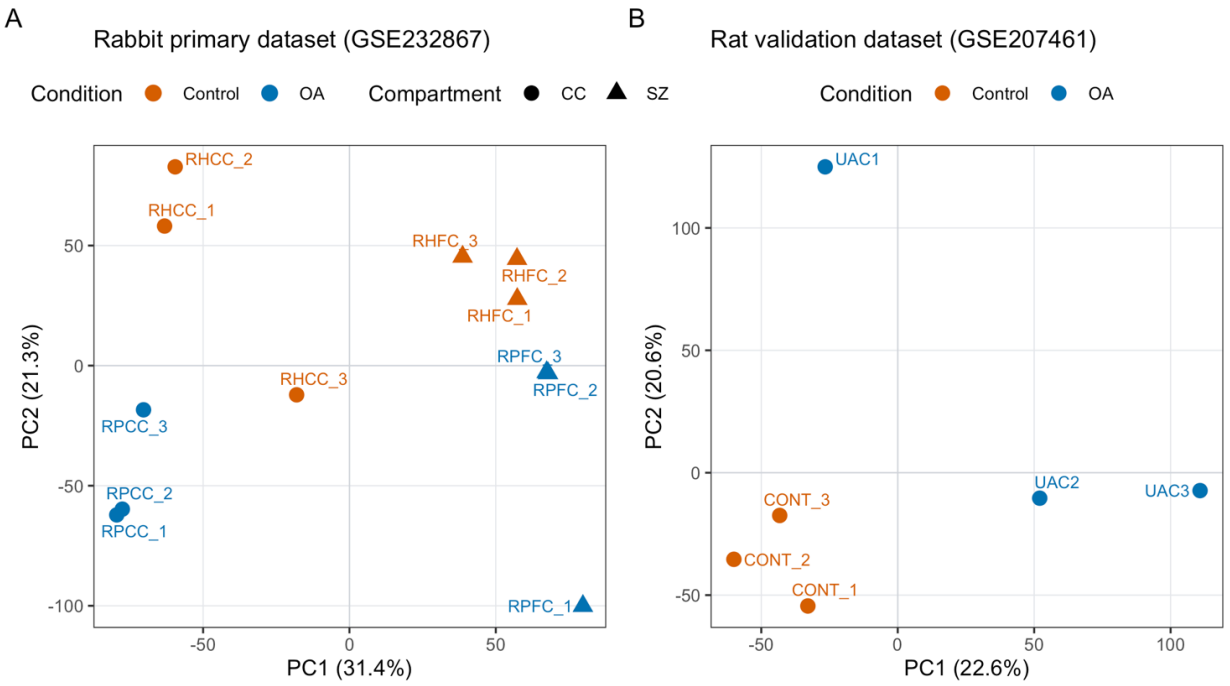

Figure 1. *Principal-component structure after TMM normalization and voom transformation. (A) Rabbit samples are shown by condition and cartilage compartment. (B) Rat samples show condition separation with one OA sample distinct on PC2. CC, condylar cartilage; OA, osteoarthritis; SZ, superficial zone; TMM, trimmed mean of M-values.*

Differential expression is extensive and compartment dependent in rabbit cartilage

Rabbit CC contained 421 differentially expressed features: 346 upregulated and 75 downregulated. Of these, 299 had gene symbols (247 upregulated and 52 downregulated). The SZ contrast contained 180 differentially expressed features (69 upregulated and 111 downregulated), and the condition-by-compartment interaction contained 135 (24 positive and 111 negative). Only one rat feature met the strict threshold.

Among the 180 threshold-positive SZ features, 135 had nonempty gene symbols. Among the 135 interaction features, 107 had symbols. The predominance of positive CC effects contrasted with the predominance of negative SZ and interaction effects. This directional asymmetry indicates that the rabbit OA response was not a uniform amplification or suppression across cartilage. Instead, many transcripts increased within CC, whereas a separate group of features decreased within SZ or showed an OA-associated change that was more negative in SZ than in CC.

The interaction result is particularly important for interpreting compartment specificity. A negative interaction does not necessarily require absolute downregulation in both compartments; it indicates that the OA effect in SZ was lower than the corresponding effect in CC. Conversely, the 24 positive interactions identify features whose OA-associated response was relatively more positive in SZ. Reporting the interaction separately from the two within-compartment contrasts prevents an apparent difference in thresholded lists from being mistaken for formal evidence of differential compartment response. The included designs and all four differential-expression summaries are detailed in Table 1. The direction and magnitude of the thresholded results, including the dominance of positive CC effects and negative SZ and interaction effects, are visualized in Figure 2.

Table 1. Included datasets and differential-expression summary.

Dataset/contrast	Tissue/model	Design	Tested	Up	Down	Total
GSE232867: OA vs control	Rabbit CC; post-traumatic	3 animals/condition	14,540	346	75	421
GSE232867: OA vs control	Rabbit SZ; post-traumatic	paired compartments	14,540	69	111	180
GSE232867: condition x compartment	Rabbit CC vs SZ response	animal block	14,540	24	111	135
GSE207461: OA vs control	Rat CC; unilateral anterior crossbite	3 samples/condition	29,815	1	0	1

CC, condylar cartilage; OA, osteoarthritis; SZ, superficial zone. Differential expression required BH-FDR <0.05 and absolute log₂ fold-change ≥1. Interaction directions refer to the SZ-minus-CC difference in OA effects.

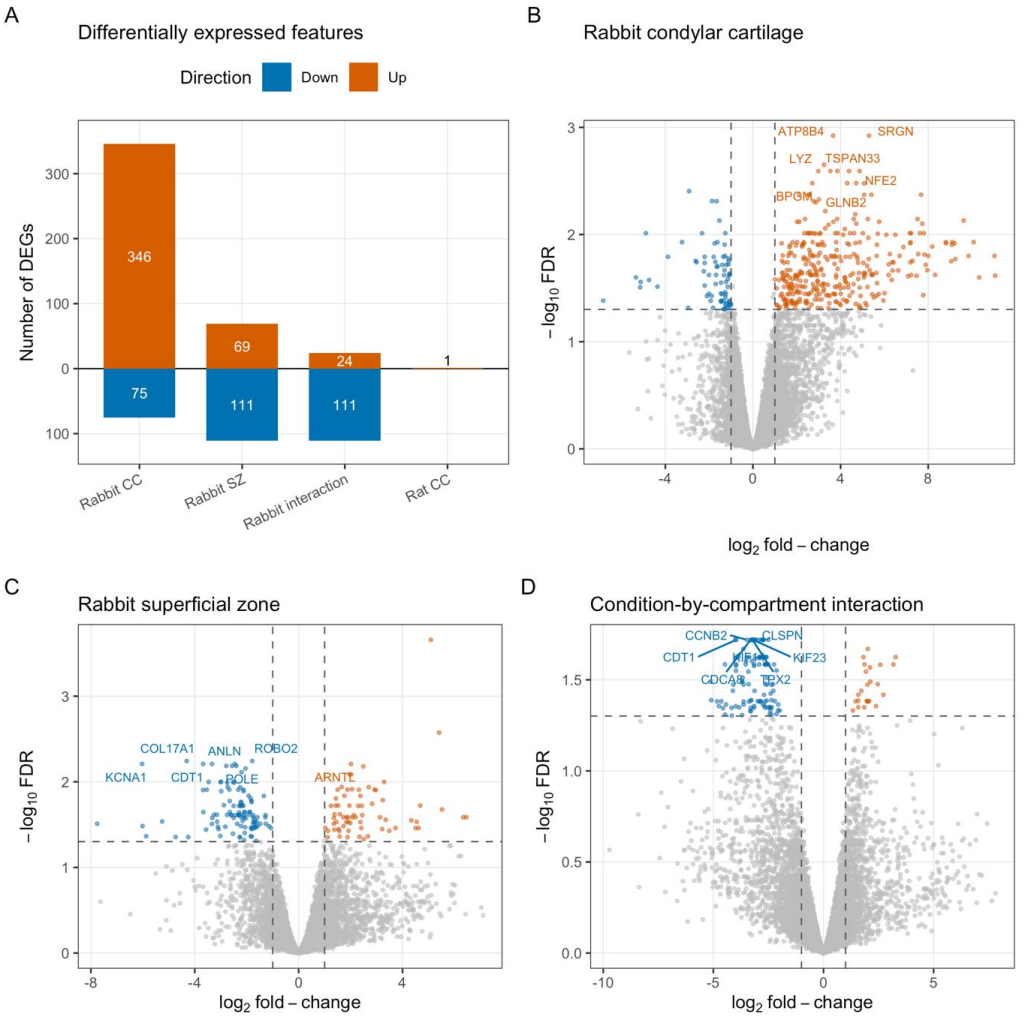

Figure 2. *Differential-expression patterns at BH-FDR <0.05 and absolute log₂ fold-change ≥1. (A) Numbers of upregulated and downregulated features. (B) Rabbit condylar-cartilage volcano plot. (C) Rabbit superficial-zone volcano plot. (D) Rabbit condition-by-compartment interaction. DEG, differentially expressed feature; FDR, false-discovery rate.*

Condylar cartilage shows an immune-associated signature

High-ranking rabbit CC genes included ATP8B4 (log₂FC 3.66; FDR 0.00120), SRGN (5.30; 0.00120), LYZ (2.98), TSPAN33 (4.38), NFE2 (4.71), ALAS2 (5.07), and VCAM1 (3.30). Coordinated increases in SRGN, LYZ, S100A8, LCN2, CYBB, and VCAM1 were compatible with innate immune activation and leukocyte recruitment. Concurrent erythroid-associated ALAS2 and BPGM signals made altered blood or cellular composition plausible.

Strict upregulated CC features were enriched for immune system process (adjusted $P=4.03 \times 10^{-18}$), immune response (2.68×10^{-11}), response to bacterium (6.82×10^{-9}), cell activation (5.64×10^{-8}), defense response (1.23×10^{-7}), and leukocyte activation (2.97×10^{-7}). Ordered downregulated signals included the TCA cycle (0.00238),

protein processing in the endoplasmic reticulum (0.0211), and N-glycan biosynthesis (0.0434).

The CC signature therefore combined several related but nonidentical components. SRGN encodes a hematopoietic proteoglycan, LYZ and LCN2 are associated with innate host-defense activity, S100A8 can mark inflammatory myeloid responses, CYBB participates in the phagocyte oxidase system, and VCAM1 is involved in leukocyte-endothelial or leukocyte-stromal adhesion. Their coordinated direction supports an immune-associated tissue state more strongly than any isolated transcript would. At the same time, the presence of erythroid-associated transcripts argues against assigning the entire signal to activated resident chondrocytes. Bulk tissue cannot determine whether these changes arose through infiltration, vascular content, local induction, or altered cell proportions.

Enrichment results reinforced the gene-level pattern by placing immune and defense categories among the most statistically supported strict CC programs. The ordered analysis also revealed a different direction of biology among negative ranks. TCA-cycle, endoplasmic-reticulum-processing, and N-glycan-biosynthesis terms passed correction despite relatively few strict downregulated CC features, illustrating the value of continuous ranks. These findings indicate coordinated decreases in transcripts related to energy metabolism and secretory processing, but they do not demonstrate metabolite concentrations, mitochondrial respiration, protein folding capacity, glycosylation products, or causal pathway inhibition. Recent transcriptomic investigations independently support the relevance of immune-associated genes and HK3-linked inflammatory metabolism in TMJ-OA [17,18].

The superficial zone shows suppression of proliferative programs

Prominent SZ decreases included COL17A1, ROBO2, CDT1, ANLN, KCNA1, TPX2, KNTC1, POLE, MCM4, and CDCA8, whereas ARNTL, GDF7, ADAMTS16, and NPAS2 increased. Downregulated SZ features were strongly enriched for mitotic cell-cycle process (adjusted $P=3.53 \times 10^{-31}$) and chromosome segregation. The interaction contrast was dominated by relative SZ suppression of TPX2, CCNB2, KIF11, KIF23, KIF15, CDT1, ANLN, CDCA8, RRM2, and CDK1. These abundance changes support compartment-specific proliferative dysregulation but do not directly measure cell-division rates.

Several of the negative SZ and interaction genes participate at different stages of the cell cycle: CDT1 and MCM4 contribute to replication licensing, POLE and RRM2 support DNA synthesis, TPX2 and kinesin-family members organize mitotic machinery, CCNB2 and CDK1 regulate entry into mitosis, and ANLN and CDCA8 contribute to cytokinesis or chromosome behavior. The convergence of multiple components makes a coordinated proliferative program more plausible than an interpretation based on one marker. However, bulk RNA abundance cannot distinguish fewer cycling cells from reduced transcription within the same cells, nor can it establish whether the affected population is a superficial progenitor-like compartment.

Positive SZ genes were fewer and represented a different biological pattern. ARNTL and NPAS2 are associated with circadian regulation, GDF7 with growth-factor signaling, and ADAMTS16 with extracellular protease biology. Recent mechanical-model profiling and experiments targeting Bmal1 or Per1 independently connect driver-gene and circadian dysregulation with TMJ-OA cartilage pathology [19,20,21]. These observations were not elevated to a single mechanistic conclusion because the strict downregulated program was substantially stronger and because functional consequences were not measured. The interaction contrast provides the clearest statistical evidence that disease effects differed by compartment, while the specific cellular explanation remains to be tested with histology, proliferation markers, or cell-resolved sequencing.

Strict gene replication is sparse but pathways replicate

Only Morf4l2 met the strict rat threshold ($\log_2$FC 2.04; FDR 0.00195). The original rat publication reported 137 mRNAs using absolute $\log_2$FC ≥1 and nominal $P<0.05$ [11]; the lower count here reflects formal FDR control. No strict DEG overlapped across species. Across 8,500 deduplicated shared symbols, $\log_2$ fold-changes showed modest positive concordance (Spearman rho=0.212; $P=2.24 \times 10^{-87}$). Because this comparison used symbols rather than curated orthologs, it was treated as supportive.

Ordered rat enrichment identified Immune System (Reactome; adjusted $P=7.26 \times 10^{-10}$), Innate Immune System (1.14×10^{-8}), neutrophil degranulation (1.20×10^{-6}), leukocyte activation (2.16×10^{-6}), and type II interferon signaling (9.71×10^{-6}). Downregulated ranks included blood-vessel development (0.00153), angiogenesis (0.00534), and ECM-receptor interaction (0.00537). Thirteen upregulated GO Biological Process terms replicated directionally across species.

The shared-symbol correlation was highly significant because it was estimated across 8,500 observations, but its magnitude was small. Statistical significance therefore should not be interpreted as close gene-by-gene agreement. The positive coefficient instead indicates a weak overall tendency for symbols with positive rabbit CC effects to have positive rat effects and for negative effects to align correspondingly. The absence of strict overlapping DEGs is consistent with the rat sample size, the heterogeneous OA cluster, and model differences, and it motivated the predefined pathway-level comparison rather than post hoc relaxation of the FDR threshold.

The 13 concordant upregulated GO terms comprised leukocyte activation, cell activation, lymphocyte activation, regulation of cell activation, regulation of leukocyte activation, defense response, response to bacterium, positive regulation of immune system process, B-cell activation, immune system process, regulation of immune system process, lymphocyte proliferation, and regulation of lymphocyte activation. Leukocyte activation had the strongest conservative evidence because both the rabbit and rat ordered analyses were significant and the larger adjusted P value was 2.16×10^{-6}. Cell activation and lymphocyte activation followed with conservative adjusted P values of 1.44×10^{-5} and 1.54×10^{-5}.

The upregulated replication pattern was therefore broader than generic inflammation: it repeatedly implicated activation and regulation of leukocyte or lymphocyte programs. By contrast, no downregulated GO Biological Process term met the same cross-species directional replication rule. Rabbit negative ranks emphasized metabolic and secretory pathways, whereas

rat negative ranks emphasized vascular development, angiogenesis, cell-junction organization, and extracellular-matrix-receptor interaction. This directional asymmetry supports a conserved immune-associated upregulated signal but indicates that the negative transcriptional response was more dependent on species, disease model, sampling, or temporal context. Independent synovial-cell and metabolite studies likewise support metabolic heterogeneity as a relevant, but compartment-dependent, dimension of TMJ-OA [22,23]. The ten strongest replicated pathways and their species-specific adjusted P values are detailed in Table 2. All 13 directionally concordant upregulated pathways and their conservative cross-species significance are visualized in Figure 3.

Table 2. Strongest directionally concordant upregulated pathways in rabbit and rat TMJ-OA cartilage.

Pathway	GO term	Rabbit adjusted P	Rat adjusted P	Conservative P*
Leukocyte activation	GO:0045321	2.45×10^{-11}	2.16×10^{-6}	2.16×10^{-6}
Cell activation	GO:0001775	5.05×10^{-12}	1.44×10^{-5}	1.44×10^{-5}
Lymphocyte activation	GO:0046649	1.54×10^{-5}	3.57×10^{-6}	1.54×10^{-5}
Regulation of cell activation	GO:0050865	2.81×10^{-5}	2.50×10^{-3}	2.50×10^{-3}
Regulation of leukocyte activation	GO:0002694	9.96×10^{-4}	2.80×10^{-3}	2.80×10^{-3}
Defense response	GO:0006952	2.98×10^{-3}	3.88×10^{-4}	2.98×10^{-3}
Response to bacterium	GO:0009617	4.09×10^{-4}	4.24×10^{-3}	4.24×10^{-3}
Positive regulation of immune system process	GO:0002684	9.17×10^{-3}	1.15×10^{-2}	1.15×10^{-2}
B-cell activation	GO:0042113	1.31×10^{-2}	1.95×10^{-3}	1.31×10^{-2}
Immune system process	GO:0002376	1.67×10^{-5}	1.61×10^{-2}	1.61×10^{-2}

**The larger adjusted P value across species. All terms were significant and enriched in the upregulated direction in both ordered analyses.*

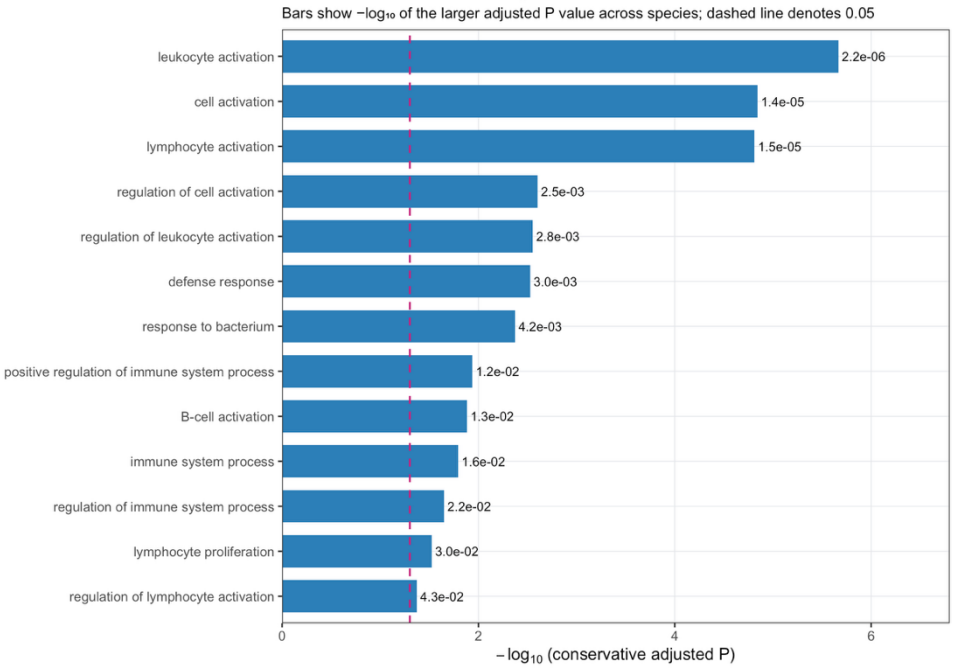

Figure 3. *Directionally concordant upregulated pathways in rabbit and rat TMJ-OA cartilage. Bars show -log[10] of the larger adjusted P value across species. The dashed line marks adjusted P=0.05. TMJ-OA, temporomandibular joint osteoarthritis.*

4. Discussion

This targeted integrative reanalysis identifies pathway-level immune activation as the most reproducible transcriptional feature across two experimentally distinct TMJ-OA cartilage models. Rabbit data provide extensive strict feature-level evidence, whereas the smaller heterogeneous rat dataset contributes primarily ranked pathway support. The result illustrates why replication should not rely exclusively on strict list overlap: coordinated subthreshold changes can preserve a biological program even when individual features do not survive multiple-testing correction.

Three findings organize the interpretation. First, rabbit condylar cartilage showed a large, predominantly upregulated disease response in which immune and defense genes formed the most coherent strict pathway signal. Second, the superficial zone showed a different directional pattern, dominated by reductions in replication, mitotic, and chromosome-segregation transcripts and supported by a formal condition-by-compartment interaction. Third, the rat dataset did not reproduce the rabbit strict DEG list, yet its ranked profile independently enriched immune, innate-immune, leukocyte-activation, and neutrophil-degranulation pathways. These layers of evidence should be interpreted together: strong within-

model effects, compartment dependence, weak gene-level cross-species correlation, and stronger functional concordance are not contradictory results but descriptions at different analytical scales.

The distinction matters for reproducibility in small transcriptomic experiments. Dichotomizing every feature at an FDR and fold-change threshold is necessary for a controlled strict list but discards information about rank and direction. When sample sizes are limited, a transcript with a similar biological effect can cross the threshold in one dataset and remain subthreshold in another because of variance, depth, annotation, or composition. Ordered enrichment does not eliminate those sources of heterogeneity, but it asks whether many members of a defined program occupy the same directional tail. The conservative requirement that a term be significant in both species prevents a single strong dataset from determining the replication claim.

Concordant leukocyte, lymphocyte, innate-immune, and neutrophil-degranulation signals agree with whole-transcriptome, single-cell, and molecular studies implicating inflammatory signaling, immune-cell participation, metabolic stress, apoptosis, and neurovascular remodeling in TMJ-OA [17,18,24-26]. Nevertheless, bulk RNA-seq cannot determine whether SRGN, LYZ, S100A8, LCN2, CYBB, and VCAM1 reflect induction within resident cells, immune-cell infiltration, vascular or blood content, or a mixture. ALAS2 and BPGM make compositional confounding particularly plausible.

Immune activation is biologically credible within current models of TMJ-OA, in which abnormal mechanical loading and tissue damage can initiate inflammatory signaling, matrix degradation, chondrocyte stress, and communication with synovial, vascular, neural, or myeloid compartments [1,2,3,27-29]. The present data add a cross-model transcriptomic perspective rather than proving a specific initiating pathway. Leukocyte activation was reproduced at the functional level, and the rat ranks also supported innate immune and type II interferon-related signaling. These patterns place immune-cartilage interaction among the most defensible candidates for further study, but they do not establish that leukocytes caused the structural degeneration or that blocking one immune pathway would reverse disease.

The cellular-composition issue deserves particular emphasis because it changes the meaning of candidate biomarkers. If elevated SRGN, LYZ, S100A8, LCN2, or CYBB primarily reflects increased abundance of infiltrating or blood-derived cells, the transcripts may be useful indicators of an inflammatory tissue state without representing chondrocyte-intrinsic targets. If VCAM1 is induced in vascular or stromal cells, it may signal altered cell adhesion or recruitment rather than cartilage-matrix regulation. Conversely, some resident condylar cells may themselves express immune-associated genes under stress. Single-cell studies in inflammatory TMJ-OA demonstrate substantial cellular diversity and support the plausibility of multiple sources, but the present bulk data cannot adjudicate among them [4,8].

This uncertainty does not invalidate the pathway finding; it defines the next experimental question. Histologic colocalization, immunostaining for myeloid and vascular markers, flow-based cell quantification, spatial transcriptomics, or matched single-cell profiling could separate changes in cell abundance from transcriptional induction. Validation should also include cartilage identity and erythroid markers so that apparently strong immune expression is not interpreted without an estimate of tissue composition. The combined presence of immune and erythroid-associated transcripts in the rabbit CC result makes such controls essential.

A second result is the compartment specificity of the rabbit response. Broad SZ decreases in DNA replication, mitosis, chromosome segregation, and cytokinesis genes may reflect impaired progenitor-like cycling or repair in the mechanically exposed surface. These transcript-abundance findings cannot establish actual proliferation rates, and validation should combine cell-cycle markers with histology or cell-resolved assays.

The formal interaction strengthens this interpretation by showing that the OA effect differed between SZ and CC for 135 features, with 111 shifted in the negative interaction direction. This is more informative than comparing two thresholded lists because it directly tests whether compartment modifies the disease response. Genes spanning replication licensing, DNA synthesis, spindle organization, motor activity, mitotic control, chromosome segregation, and cytokinesis were represented. Such breadth is consistent with coordinated cell-cycle dysregulation rather than a single-gene anomaly, although the direction could arise from fewer cycling cells, altered maturation, tissue loss, or decreased transcription per cell.

The superficial zone has a distinctive mechanical and reparative role, so reduced proliferative-program representation may be relevant to surface maintenance. A diminished capacity to renew or organize the exposed layer could plausibly contribute to failed repair after injury. However, this remains a hypothesis, not a measured regenerative endpoint. The study did not include bromodeoxyuridine incorporation, Ki-67 staining, cell counts, lineage tracing, histomorphometry, or longitudinal sampling. Future experiments should test whether the transcriptomic pattern corresponds to reduced proliferation, altered cell-cycle phase distribution, senescence, apoptosis, or depletion of a specific superficial population.

The smaller group of positive SZ transcripts may represent compensatory or temporally distinct programs. Circadian regulators, growth-factor-related transcripts, and extracellular protease genes could reflect an attempted adaptive response to mechanical disruption. Because these signals were fewer and were not supported by a single dominant enrichment theme, they should not be combined into a definitive mechanism. Their value lies in generating focused hypotheses that can be tested alongside the stronger negative cell-cycle program.

The CC data also suggest reduced TCA-cycle representation and disturbed endoplasmic-reticulum processing and N-glycan biosynthesis. These pathways are compatible with energetic and secretory stress but do not establish metabolic flux, protein abundance, or causality. Rat downregulation of angiogenesis and ECM-receptor interaction may reflect model timing, compartment composition, or a different repair state.

Metabolic and secretory pathways are relevant to cartilage because matrix-producing cells must coordinate energy supply, protein synthesis, folding, processing, and

extracellular export. A coordinated negative rank in TCA-cycle or endoplasmic-reticulum-related genes may therefore accompany a stressed or less biosynthetically active tissue state. Integration of metabolomic and transcriptomic evidence has likewise been proposed as a way to characterize TMJ-OA mechanisms [12,22,23,25,26]. Nevertheless, transcript ranks are several steps removed from metabolic activity. Targeted metabolite measurements, oxygen-consumption assays, mitochondrial imaging, proteomics, and glycomic analyses would be required to establish functional impairment.

The rat negative profile differed substantially, emphasizing blood-vessel development, angiogenesis, junction organization, and ECM-receptor interaction. Several explanations are compatible with the data. Mechanical-malocclusion disease at eight weeks may represent a different stage from post-traumatic rabbit disease; tissue dissection may capture different proportions of vascular or osteochondral compartments; and annotation or power may change which negative ranks dominate. Because no downregulated pathway met the cross-species replication rule, these findings should be treated as model-specific context rather than as a conserved anti-angiogenic response.

Selection was intentionally role based rather than exhaustive. Of 34 candidate GEO records, most represented single-cell/spatial data, non-cartilage tissues, in-vitro systems, mechanism-specific genetic or treatment experiments, parent accessions, or under-replicated contrasts. This restriction improved comparability but also means the conclusions apply to the two selected models rather than the complete TMJ-OA transcriptomic literature and should be prospectively tested in additional public datasets.

Role-based selection reduced one form of heterogeneity while introducing a clear boundary on generalizability. The analysis does not summarize every TMJ-OA tissue, intervention, genetic model, or omics platform. It is not a systematic review and cannot estimate the prevalence of a pathway across the literature. Its contribution is narrower: among currently accessible, replicated bulk count datasets that fulfilled the specified analytical roles, it identifies a pathway-level signal shared by two species and a compartment-specific signal supported within the paired rabbit design. Replication in future human and animal datasets remains necessary.

Translational implications

The conserved immune program prioritizes SRGN, LYZ, S100A8, LCN2, CYBB, and VCAM1 for validation alongside cartilage-matrix and cell-identity markers. Quantitative reverse-transcription PCR and immunohistochemistry in independent tissue should be paired with histologic scoring and immune-cell markers. Single-cell or spatial transcriptomics could locate signals in infiltrating leukocytes, vascular cells, superficial-zone populations, or resident chondrocytes [4,8]. Extracellular-vesicle studies illustrate parallel efforts to modify immune and osteoclast components of the TMJ-OA microenvironment [30-,32].

A useful validation sequence would begin with independent bulk tissue collected under a prespecified dissection protocol, followed by targeted confirmation of both immune-associated and cell-cycle-associated transcripts. Protein-level localization should then determine whether candidate signals occur in cartilage cells, synovial or vascular structures, or infiltrating immune populations. Pairing these measurements with standardized structural scoring would test whether expression tracks tissue severity. A longitudinal design could further distinguish early inflammatory responses from later degeneration or repair failure.

Translation to human disease should be approached as a staged process rather than as immediate biomarker or therapeutic development. Human condylar cartilage is difficult to obtain from healthy controls, and surgical tissue can represent advanced disease and treatment selection. Synovial fluid, blood, or saliva may be more accessible but cannot be assumed to reproduce cartilage expression. Candidate markers should first demonstrate tissue and cellular specificity, analytical reproducibility, and an association with clinically relevant phenotypes before diagnostic or prognostic performance is considered.

Therapeutic interpretation also requires caution. Immune-associated pathways could contain damaging, compensatory, or repair-supporting components, and broad suppression might have different effects across disease stages. Experimental perturbation should therefore be pathway and cell-type specific. Recent siRNA delivery, Wnt16 microgel, Syndecan-4 inhibition, and DDIT3-targeted mechanistic studies illustrate the expanding therapeutic landscape, but the present observational transcriptomic analysis does not identify an effective treatment or establish target causality [33-36].

Strengths and limitations

Strengths include direct recovery of deposited count matrices, explicit modeling of paired rabbit compartments, empirical-Bayes inference with FDR control, protein-coding enrichment backgrounds, directional cross-species testing, and a fully packaged computational audit trail. The analysis preserves study-specific effects rather than pooling nonexchangeable models.

Additional strengths arise from consistency of the inferential framework. Both species underwent design-aware low-expression filtering, TMM normalization, voom precision weighting, trend-moderated limma modeling, and Benjamini-Hochberg correction. The rabbit interaction formally tested compartment modification, while duplicate correlation represented within-animal dependence. Strict and ordered enrichment were separated, species-specific detectable backgrounds were used, and pathway replication required significance and matching direction in both datasets. Complete feature-level tables make it possible to inspect results beyond the selected displays.

The recovery of the malformed rabbit worksheet dimension is also relevant to reproducibility. A routine spreadsheet reader returned only the declared A1 cell even though the workbook contained a complete matrix. Reading the explicit populated range, reconciling its headers with GEO metadata, and retaining the original file allowed the analysis to use the deposited counts without manual transcription. Documenting this step protects against an otherwise silent data-loss error and makes the derived totals auditable.

Limitations are substantial. Both datasets had only three biological replicates per condition. Species, disease induction, timing, and dissection differed. Bulk tissue confounds cell-intrinsic regulation with cell-proportion shifts. Enrichment depends on annotation and ranked-list

choices. Symbol matching does not replace curated orthology, and the significant cross-species correlation was modest. The selection was targeted rather than a registered systematic integration. Finally, the findings are preclinical because human condylar-cartilage validation was unavailable.

The sample sizes constrain variance estimation, outlier assessment, and generalizability. Empirical-Bayes moderation improves stability but cannot create biological replication that is absent. One rat OA sample was separated on PC2; retaining it avoids subjective exclusion, yet the resulting within-group heterogeneity reduces strict power. The rabbit design contains only six animals even though 12 tissue profiles were measured, so the number of independent biological units is smaller than the number of columns in the matrix. No prospective sample-size calculation or independent confirmatory cohort was available for this secondary analysis.

Cross-species symbol integration is another important limitation. Case-insensitive shared symbols offer a transparent supportive comparison, but they may combine paralogs, omit species-specific genes, or fail to represent one-to-many orthology. Deduplication by the largest absolute moderated t statistic prevents repeated symbols from receiving multiple weight but can favor the most extreme mapped row. A curated orthology analysis could refine feature-level correspondence, although it would not remove differences in anatomy, induction, sampling, or experimental timing.

Functional enrichment inherits limitations from database content and term dependence. GO categories overlap hierarchically, related immune terms share many genes, and g:SCS-adjusted significance does not make each term an independent biological discovery. The ordered query size of 5,000 captures broad rank information but is still an analytical choice. The custom background reduces detection bias, and the dual-species rule increases stringency, yet enrichment cannot establish pathway activity, causal direction, or cellular location.

Finally, the analysis relies on deposited gene-level counts and metadata rather than raw-read reprocessing. This preserves the source quantification but prevents independent evaluation of alignment quality, transcript assignment, batch effects arising before deposition, or alternative genome builds. Clinical data, sex-stratified effects, detailed histologic severity, and harmonized time-course measurements were not available for integrated modeling. These residual limitations make the findings most appropriate as reproducible, hypothesis-generating evidence for conserved immune activation and compartment-specific dysregulation.

5. Conclusion

Across two independent animal TMJ-OA cartilage datasets, upregulated immune and leukocyte-activation pathways were the most consistently replicated transcriptional programs. Rabbit cartilage additionally showed strong compartment dependence: condylar cartilage had extensive immune-associated and metabolic dysregulation, whereas the superficial zone showed suppression of proliferative and chromosome-segregation programs. These observations nominate immune-cartilage interactions and superficial-zone repair failure as testable mechanisms, but they remain hypothesis-generating until confirmed in additional models, cell-resolved assays, and human condylar cartilage.

The study also demonstrates that reproducibility can be evaluated without pooling incompatible experiments: strict feature-level inference, a formal compartment interaction, supportive shared-symbol concordance, and conservative directional pathway replication provide complementary evidence. Future work should verify cellular sources, relate expression to structural severity and disease stage, apply curated orthology, and test the nominated programs in independent human and animal tissues before biomarker or therapeutic claims are made.

Declarations

Ethics approval and consent to participate: Not applicable. This secondary analysis used publicly available, de-identified transcriptomic data. Ethical oversight for animal procedures was reported by the investigators of the original studies.

Consent for publication: Not applicable.

Conflict of interest: The authors declare that they have no known competing financial interests or personal relationships that could have influenced the work reported in this article.

Funding: This research received no specific grant from any funding agency in the public, commercial, or not-for-profit sectors.

Author contributions (CRediT): DS: Conceptualization, methodology, software, formal analysis, investigation, data curation, visualization, writing - original draft, and project administration. CS: Methodology, validation, investigation, data curation, and writing - review and editing. VS: Validation, visualization, supervision, and writing - review and editing. All authors reviewed and approved the final manuscript and accept responsibility for the integrity of the work.

Data and code availability: Primary data are publicly available from NCBI GEO under GSE232867 and GSE207461. The accompanying supplementary archive contains analysis scripts, complete differential-expression and enrichment outputs, API responses, screening records, figure files, and R session information.

Acknowledgments: The authors thank the investigators who generated and deposited the GEO datasets and acknowledge NCBI GEO for maintaining public access to transcriptomic data.

Use of artificial intelligence: The authors declare that no generative artificial intelligence tools were used in the conceptualization, analysis, writing, editing, or preparation of this manuscript.

References

1. Feng X, Li S, Wang S, et al. Piezo1 mediates the degradation of cartilage extracellular matrix in malocclusion-induced TMJOA. Oral Dis. 2024;30(4):2425-2438. doi: 10.1111/odi.14615.
2. Zou Y, Huang P, Lin H, et al. The dynamic progression of temporomandibular joint osteoarthritis-like lesions elicited by mandibular shift in a rat model. Ann Anat. 2024;255:152301. doi: 10.1016/j.aanat.2024.152301.
3. Xing L, Qi X, Wu J, et al. Histopathological characterization of mandibular condyles in four temporomandibular joint osteoarthritis mouse models. Arch Oral Biol. 2025;170:106129. doi: 10.1016/j.archoralbio.2024.106129.
4. Zhang D, Zhang Y, Xia S, et al. Single-cell RNA sequencing reveals neurovascular-osteochondral network crosstalk during temporomandibular joint osteoarthritis: pilot study in human condylar cartilage. Heliyon. 2023;9(10):e20749. doi: 10.1016/j.heliyon.2023.e20749.
5. Wang J, Dong X, Lei J, et al. β-catenin orchestrates Gli1+ cell fate in condylar development and TMJOA. J Dent Res. 2024;103(12):1291-1301. doi: 10.1177/00220345241274354.

6. Zhu M, Huang Z, Qin J, et al. Loss of β-arrestin2 aggravated condylar cartilage degeneration at the early stage of temporomandibular joint osteoarthritis. BMC Musculoskelet Disord. 2024;25(1):451. doi: 10.1186/s12891-024-07558-z.
7. Kang X, Liu Q, Shi Y, et al. Decreased expression of ATP-binding cassette protein G1 promotes abnormal adipogenesis of condylar chondrocytes in temporomandibular joint osteoarthritis. J Oral Rehabil. 2024;51(5):805-816. doi: 10.1111/joor.13647.
8. Jariyasakulroj S, Shu Y, Lin Z, et al. Mapping cell diversity and dynamics in inflammatory temporomandibular joint osteoarthritis with pain at single-cell resolution. JCI Insight. 2025;10(3):e184379. doi: 10.1172/jci.insight.184379.
9. Chen BY, Pathak JL, Lin HY, et al. Inflammation triggers chondrocyte ferroptosis in TMJOA via HIF-1α/TFRC. J Dent Res. 2024;103(7):712-722. doi: 10.1177/00220345241242389.
10. Tosa I, Ruscitto A, Wang Z, et al. Bulk RNA-seq analyses of mandibular condylar cartilage in a post-traumatic TMJ osteoarthritis rabbit model. Orthod Craniofac Res. 2023;26(Suppl 1):131-141. doi: 10.1111/ocr.12649.
11. Wu F, An Y, Zhou L, et al. Whole-transcriptome sequencing and ceRNA interaction network of temporomandibular joint osteoarthritis. Front Genet. 2022;13:962574. doi: 10.3389/fgene.2022.962574.
12. Tuerxun P, Ng T, Zhao K, et al. Integration of metabolomics and transcriptomics provides insights into the molecular mechanism of temporomandibular joint osteoarthritis. PLoS One. 2024;19(5):e0301341. doi: 10.1371/journal.pone.0301341.
13. Al Turkestani N, Li T, Bianchi J, et al. A comprehensive patient-specific prediction model for temporomandibular joint osteoarthritis progression. Proc Natl Acad Sci U S A. 2024;121(8):e2306132121. doi: 10.1073/pnas.2306132121.
14. Robinson MD, McCarthy DJ, Smyth GK. edgeR: a Bioconductor package for differential expression analysis of digital gene expression data. Bioinformatics. 2010;26(1):139-140. doi: 10.1093/bioinformatics/btp616.
15. Law CW, Chen Y, Shi W, et al. voom: precision weights unlock linear model analysis tools for RNA-seq read counts. Genome Biol. 2014;15(2):R29. doi: 10.1186/gb-2014-15-2-r29.
16. Ritchie ME, Phipson B, Wu D, et al. limma powers differential expression analyses for RNA-sequencing and microarray studies. Nucleic Acids Res. 2015;43(7):e47. doi: 10.1093/nar/gkv007.
17. Zhu M, Xing M, Sun R, et al. Identification of potential immune-related genes and infiltrations in temporomandibular joint osteoarthritis. Ann Med Surg (Lond). 2024;86(12):7135-7146. doi: 10.1097/MS9.0000000000002682.
18. Luo P, Lv X, Wan W, et al. Identification of HK3 as a potential key biomarker in the progression of temporomandibular joint osteoarthritis via RNA sequencing. Biology (Basel). 2025;14(11):1492. doi: 10.3390/biology14111492.
19. Liu S, Wu C, Yao Y, et al. Single monoiodoacetic acid injection reveals toll-like receptor, oestrogen, oxidative stress, and altered energy metabolism as key drivers of temporomandibular joint osteoarthritis in female rats. Arch Oral Biol. 2025;174:106233. doi: 10.1016/j.archoralbio.2025.106233.
20. Liao L, Yang L, Li Y, et al. Deletion of Bmal1 in aggrecan-expressing cells leads to mouse temporomandibular joint osteoarthritis. J Bone Miner Metab. 2024;42(5):529-537. doi: 10.1007/s00774-024-01524-4.
21. Wei J, Wang Y, Tu S, et al. Circadian rhythm disruption upregulating Per1 in mandibular condylar chondrocytes mediating temporomandibular joint osteoarthritis via GSK3β/β-catenin pathway. J Transl Med. 2024;22(1):662. doi: 10.1186/s12967-024-05475-2.
22. Zhang D, Zhang Y, Xia S, et al. Metabolic profiling of synovial fluid in human temporomandibular joint osteoarthritis. Front Immunol. 2024;15:1335181. doi: 10.3389/fimmu.2024.1335181.
23. Song Z, Xu Y, Li C, et al. Association of glutamine metabolites in synovial fluid with the severity of temporomandibular joint osteoarthritis. BMC Musculoskelet Disord. 2025;26(1):653. doi: 10.1186/s12891-025-08898-0.
24. Tang H, Ma C, Xu M, et al. SGK1 triggers cartilage degradation in TMJOA via FoxO1/autophagy. Arthritis Res Ther. 2025;27(1):231. doi: 10.1186/s13075-025-03690-w.
25. Zhao J, Li R, Du T, et al. USP32 promotes temporomandibular joint osteoarthritis by modulating PKM2 stability and glycolytic metabolism in chondrocytes. Cell Death Dis. 2025;16(1):781. doi: 10.1038/s41419-025-08053-6.
26. Dong Y, Zhou X, Zhang Z, et al. cGAS-STING aggravates cartilage degradation by promoting glycolysis in temporomandibular joint osteoarthritis. J Bone Miner Res. 2025;40(5):699-709. doi: 10.1093/jbmr/zjaf029.
27. Liu X, Luo X, Xiao M, et al. TREM2 activation relieves TMJOA by stabilizing the synovial barrier via Siglec1. J Dent Res. 2025;104(9):1003-1013. doi: 10.1177/00220345251320946.
28. Yan B, Li Y, Liu Y, et al. Targeted soluble epoxide hydrolase inhibits M1 macrophage polarization to improve cartilage injury in temporomandibular joint osteoarthritis. J Transl Med. 2025;23(1):969. doi: 10.1186/s12967-025-07003-2.
29. Jia X, Liu X, Zhu T, et al. Infiltrated macrophages aggravate TMJOA chronic pain via Piezo2 in IB4+-TG neurons. Oral Dis. 2025;31(6):1841-1853. doi: 10.1111/odi.15304.
30. Mei Z, Li H, Huang C, et al. Extracellular vesicles from adipose-derived stromal/stem cells reprogram dendritic cells to alleviate rat TMJOA by transferring mitochondria. J Nanobiotechnology. 2025;23(1):389. doi: 10.1186/s12951-025-03478-9.
31. Diez-Guardia V, Tian Y, Guo Y, et al. Controlled release of human dental pulp stem cell-derived exosomes from hydrogels attenuates temporomandibular joint osteoarthritis. Adv Healthc Mater. 2025;14(31):e2402923. doi: 10.1002/adhm.202402923.
32. Yang Z, Zhang S, Faqeer A, et al. Mesenchymal stem cell-derived extracellular vesicles ameliorate temporomandibular joint osteoarthritis by suppressing osteoclast activity via let-7a-5p/integrin β3 axis. ACS Nano. 2025;19(39):34928-34941. doi: 10.1021/acsnano.5c11211.
33. Liao S, Liu Z, Lv W, et al. Efficient delivery of siRNA via tetrahedral framework nucleic acids: inflammation attenuation and matrix regeneration in temporomandibular joint osteoarthritis. ACS Appl Mater Interfaces. 2024;16(40):53499-53514. doi: 10.1021/acsami.4c11089.
34. Zhu Y, Cao L, Yuan M, et al. Microgel encapsulated mesoporous silica nanoparticles for releasing Wnt16 to synergistically treat temporomandibular joint osteoarthritis. Adv Sci (Weinh). 2024;11(41):e2404396. doi: 10.1002/advs.202404396.
35. Chen X, He F, Zhang H, et al. Syndecan-4 inhibition attenuates cartilage degeneration in temporomandibular joint osteoarthritis. J Oral Rehabil. 2024;51(11):2324-2335. doi: 10.1111/joor.13829.
36. Yang C, Dong W, Wang Y, et al. DDIT3 aggravates TMJOA cartilage degradation via Nrf2/HO-1/NLRP3-mediated autophagy. Osteoarthritis Cartilage. 2024;32(8):921-937. doi: 10.1016/j.joca.2024.04.017.